JMEPEG (2012) 21:951–957
DOI: 10.1007/s11665-011-0003-4

1059-9495/$19.00

Combustion Synthesis in a Mechanically Activated Mg-C-TiO_2-H_3BO_3 System

B. Aminikia, S.A. Tayebifard, and A.A. Youzbashi

(Submitted April 1, 2011; in revised form June 29, 2011)

TiC-TiB_2 nanocomposite was fabricated by self-propagating high-temperature synthesis (SHS) of mechanically milled powders. H_3BO_3, TiO_2, Mg, and C as starting materials were milled for 0.5, 1, and 3 h then pressed to form pellets. Green compacts were placed in a tube furnace which had been preheated to three different temperatures of 900, 1000, and 1100 °C with argon atmosphere, for the synthesis. The prepared samples were studied by XRD, SEM, and TEM analytical technique. TiC and TiB_2 were not formed during milling process. According to the XRD patterns of synthesized samples, ball milling for 0.5 h is the optimum time for mechanical activation of the mixed powders. Further investigation indicated that 900 °C is the best temperature for the synthesis of this mixture. By using Williamson-Hall method, the average crystallite sizes of TiB_2 and TiC were calculated 40.7 and 75.6 nm, respectively, which were confirmed by TEM images.

Keywords mechanical activation, SHS, titanium carbide, titanium diboride

1. Introduction

Titanium diboride and titanium carbide, due to their high melting point, hardness, good thermal shock resistance and high-temperature stability, constitute an excellent choice for the applications in high performance cutting tools and abrasives, wear resistant parts and armored vehicles (Ref 1). These properties along with their light weight make them attractive in aircraft propulsion systems and space vehicle thermal protection, too (Ref 2). Self-propagating high-temperature synthesis (SHS), also termed as combustion synthesis (CS) developed by Merzhanov and Borovinskaya in the late 1960s (Ref 3, 4), has been expanding during the last several decades due to its attractive merits of high purity products, low processing cost, time and energy saving, low-temperature furnace, and nonpolluting process (Ref 3-5). It is therefore, used as a new technique for the synthesis of ceramics, intermetallics, ceramic matrix composites (CMCs), metal matrix composites, and so on (Ref 3, 6). However, a major limitation in the application of SHS reactions to the production of advanced material components is the inherent high porosity, e.g., the synthesized materials typically have 50% of the theoretical density (Ref 3). In order to increase the reactivity of the green powders a ball milling (MA) process can be used prior to the SHS reaction. The use of mechanical activation prior to the SHS process can result in the formation of nanostructured materials (Ref 7).

In this study, therefore, formation of nano-crystalline TiB_2-TiC composite by MASHS process, using inexpensive raw materials, such as boric acid (H_3BO_3), titanium oxide (TiO_2), graphite and Mg as reducing agent, was investigated. The reaction occurring in this process can be written as follows:

$$2H_3BO_3 + 2TiO_2 + 7Mg + C = TiC + TiB_2 + 7MgO + 3H_2O$$
$$\Delta H^{\circ}_{298} = -1512\ \text{kJ/mol} \quad \text{(Eq 1)}$$

However, since during the process H_3BO_3 melts at 139 °C and subsequently at 169 °C it dissociates into B_2O_3 and H_2O (Ref 8). Mg plays the major role in this reduction process; however, carbothermic reduction also may occur. Due to the high exothermic enthalpy of this reaction [−1512 kJ/mol, as calculated from the data compiled by Turkdogan (Ref 9)], it can be carried out either in a tube furnace at 1300-1500 K or by partial ignition of the reactant mixture, which then becomes self-sustaining (Ref 10, 11). MgO and these components formed in the products through this CS technique can be easily removed from the products by being leached in dilute HCl solution (Ref 12, 13).

2. Experimental

TiO_2 (Merck Chemicals, 99% pure, particle size <40 μm), H_3BO_3 (Merck Chemicals, 99% pure, particle size <60 μm), graphite (Merck Chemicals, 99% pure, particle size <40 μm), and Mg (Merck Chemicals, 99.95% pure, particle size <150 μm) were used as the starting materials. The powders were mixed in accordance with the stoichiometry given by Eq 1. Ball milling of the powder mixture was carried out at room temperature in a planetary ball mill. The necessary information about this process is shown in Table 1. The cups were evacuated and filled with pure argon gas to prevent oxidation during the milling process. The MA process was performed at different milling times (0.5, 1, and 3 h) using a planetary mill with blend of hardened steel balls (10 and 20 mm diameters) and the samples were designated as A_1, A_2, and A_3, respectively. No process control agent (PCA) was used, since; H_3BO_3 is able to reduce the agglomeration (Ref 14). After the milling process,

B. Aminikia, S.A. Tayebifard, and **A.A. Youzbashi**, Materials and Energy Research Center (MERC), Alvand Street, Tehran 14155-4777, Iran. Contact e-mail: behzad_aminikia@yahoo.com.

the mixture was oven-dried at 90 °C for 4 h. The dried powders were then passed through a 100-mesh sieve to reduce the number of agglomerates. The powder mixtures were uniaxially pressed in a stainless steel die at about 300 MPa without a binder into a cylindrical compact of about 10 mm diameter and 5 mm height. The initial density of the green compacts was estimated from the mass and geometry to be about 70% of the theoretical density of the reactants. The green samples were put in a tube furnace which preheated to three different temperatures 900, 1000, and 1100 °C for the CS process. Structural changes of the powders were studied by x-ray diffraction (XRD) (mod.PW1830, Philips Analytical B.V, the Netherlands) with Cu K_α radiation and Ni filter. The powders morphology was investigated by scanning electron microscopy (SEM) (mod.XL30, Philips, the Netherlands at an acceleration voltage of 30 kV). The sample for transmission electron microscopy (TEM) was prepared by suspending the powder sample in ethanol and subjecting it to ultrasonic vibration to break up aggregates. A drop of the suspension was then placed on a carbon-coated copper grid and dried. The sample powder mounted on the copper grid was then studied using a 100 kV Philips EM208S transmission electron microscope.

3. Results and Discussion

3.1 Morphological Studies

The XRD patterns of the as-milled samples are shown in Fig. 1 These patterns demonstrate that no reaction has taken place during the milling process, as the patterns include only the peaks which are assigned to the reactants. The only important change that is worth mentioning is the intensity reduction of the main peak of H_3BO_3 for sample A_3 (about $2\theta = 28°$), which might be due to the moisture removal from the H_3BO_3. If the temperature rises to above 120 °C because of the intensive ball-to-ball and ball-to-powder collisions, the H_3BO_3 will be dehydrated to some extent and boron oxide will be produced. It should be mentioned that in the microscopic scale, the reaction between the reactants could occur several times during the milling where, considerable amount of heat may be released to increase the local temperature.

Table 1 Details of ball machine and milling conditions

Rotation speed of disc, rpm	250
Cup material	Hardened chromium steel
Capacity of cup, mL	150
Ball material	Hardened carbon steel
Diameter of balls, mm	10-20
Number of balls	15
Balls to powder weight ratio	15:1
Total powder mass, g	15

Synthesized samples had a fragile sponge-like structure and they could easily be ground by an agate mortar and pestle. In powder form, they were subject to XRD analyses. Figures 2-4 show the XRD patterns of the typical products which were synthesized in 900, 1000, and 1100 °C, respectively. However, it has been reported that during the Eq 1, side reactions take place leading to the formation of Mg_2TiO_4 and $Mg_3B_2O_6$ products (Ref 15). However, according to the Eq 1, only TiC, TiB_2, and MgO were expected as products. It could be seen that, in addition to these major phases, other minor phases such as Mg_2TiO_4 and $Mg_3B_2O_6$ were also present as shown in Figs. 2-4. Formation of Mg_2TiO_4 and $Mg_3B_2O_6$ minor phases may be caused by the reaction between unreacted TiO_2 and B_2O_3, with formed MgO according to the following reactions:

$$TiO_2 + 2MgO = Mg_2TiO_4 \quad \Delta G^\circ = -12.2 \text{ kJ} \qquad \text{(Eq 2)}$$

$$B_2O_3 + 3MgO = Mg_3B_2O_6 \quad \Delta G^\circ = -153 \text{ kJ} \qquad \text{(Eq 3)}$$

by increasing the energy level of the reactants via mechanical activation (MA) of the powders, the reactivity of the reactants increases, resulting in a higher conversion of reactants to the side products. This phenomenon is clearly seen in Figs. 2(c), 3(c), and 4(c). Hence, according to these figures, milling of the reactants for 0.5 h is the optimum time for mechanical activation of the powders. MgO and other components of the undesired products can be removed by leaching in dilute HCl solution.

Figure 5 shows SEM micrographs of products obtained through the SHS reaction. It is clearly seen that by increasing the temperature, grain growth greatly increases and the grains are angular and flaky in shape. It is worth mentioning that the other effect of raising the temperature is the increase of porosity

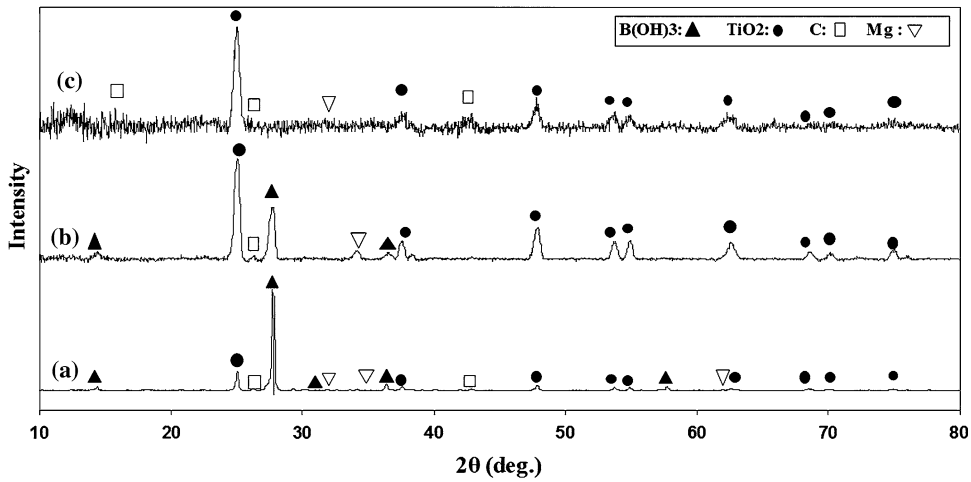

Fig. 1 XRD patterns taken from the mixtures after (a) 0.5 h, (b) 1 h, and (c) 3 h of milling times

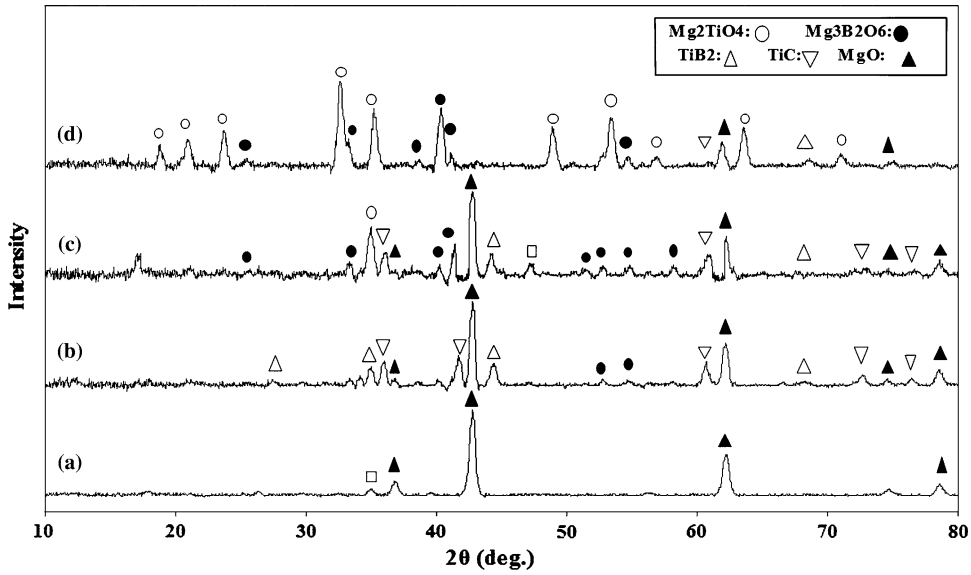

Fig. 2 XRD patterns of the samples with (a) as-received, (b) 0.5 h, (c) 1 h, (d) 3 h and synthesized in 900 °C

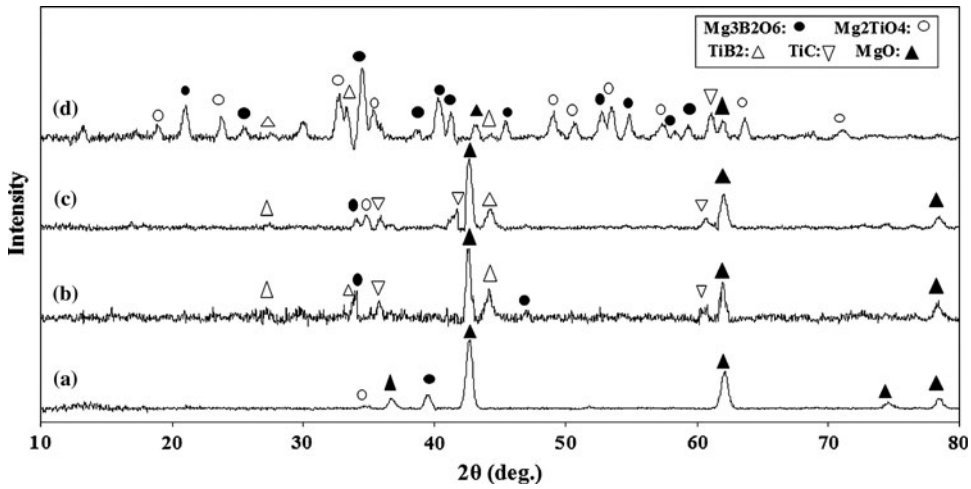

Fig. 3 XRD patterns of the samples with (a) as-received, (b) 0.5 h, (c) 1 h, (d) 3 h and synthesized in 1000 °C

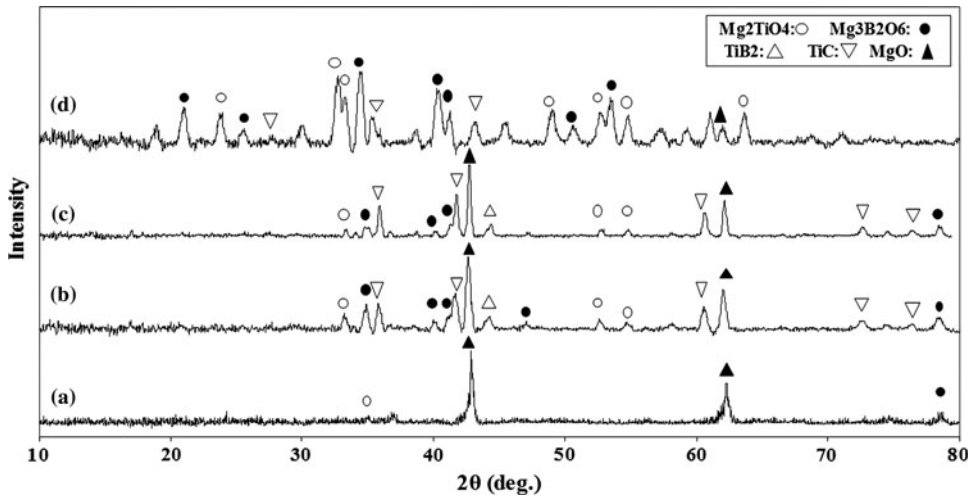

Fig. 4 XRD patterns of the samples with (a) as-received, (b) 0.5 h, (c) 1 h, (d) 3 h and synthesized in 1100 °C

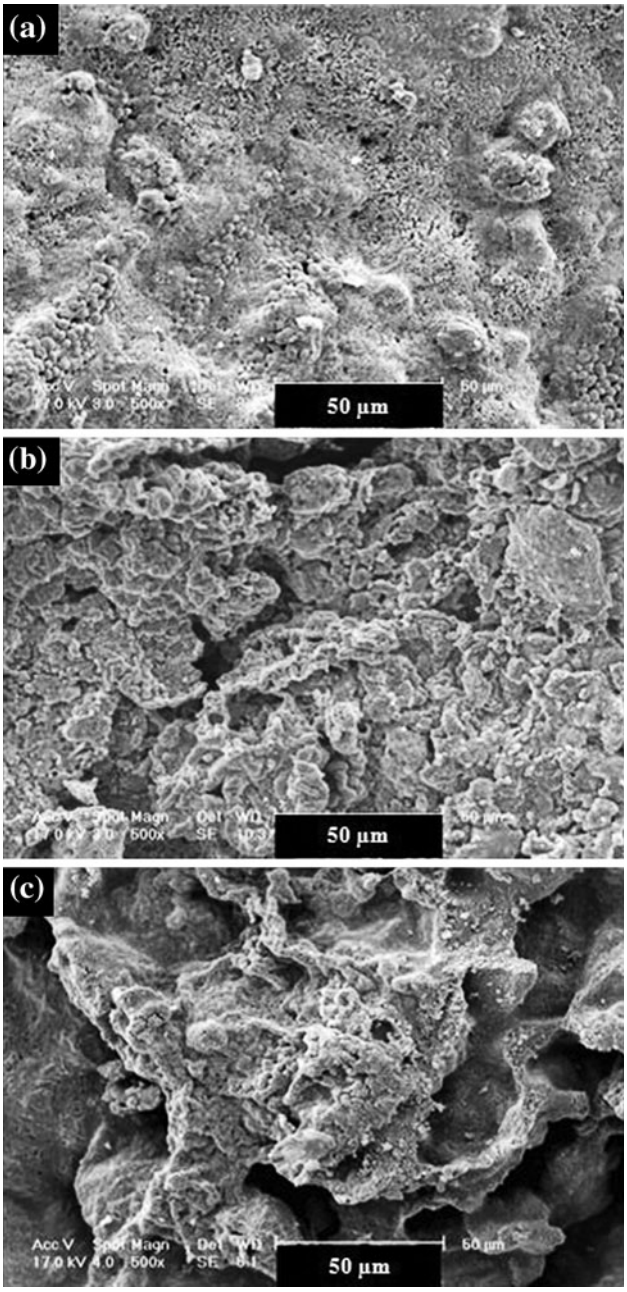

Fig. 5 SEM micrographs of products synthesized in (a) 900 °C, (b) 1000 °C, and (c) 1100 °C (500×)

and locally shrinkage of grains due to the formation of liquid phase in high temperatures (Ref 16). So that, in sample which was milled for 0.5 h and was synthesized at 1100 °C, grains have been formed in an irregular surface and especially in coarse-shaped agglomerates. According to the XRD analyses, these aggregates are composed of mainly MgO, TiC, and TiB_2 and minor amount of Mg_2TiO_4 and $Mg_3B_2O_6$ phases. The morphological study of the products indicates the agglomeration of the oxide compounds along with TiC and TiB_2. Among the synthesized samples, A_1 showed to be the most desired product as TiC and TiB_2 could be readily formed, whereas, in other cases, the desired products could not be completely formed. The elongated or rectangular particulates are TiB_2, whereas the nearly spherical particulates are TiC (Fig. 6). These

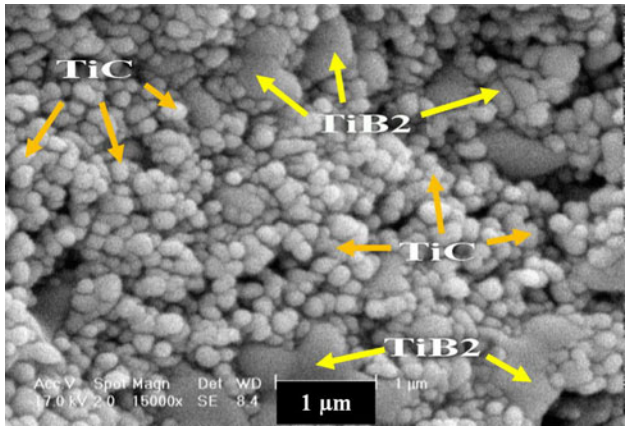

Fig. 6 SEM micrograph of products synthesized in 900 °C (15,000×): the rectangular particulates are TiB_2 and the spherical particulates are TiC

particulates morphologies were similar to those observed for monolithic TiB_2 and TiC (Ref 6). Therefore, the product sample A_1 was chosen to undergo leaching step, in order to wash away the side reaction products.

3.2 Thermodynamic Analysis

An important thermodynamic parameter in this regard is the adiabatic temperature of reaction (T_{ad}) which is the maximum temperature achieved under adiabatic conditions as a consequence of the evolution of heat from the reaction. It has been suggested that the value of T_{ad} should be above 1800 K to yield self-propagating combustion reaction in a thermally ignited system (Ref 17, 18). The value of T_{ad} can be calculated using following equation:

$$-\Delta H^{\circ}_{298} = \int_{T_0}^{T_{ad}} \Delta C_p dT \qquad \text{(Eq 4)}$$

where ΔH°_{298} is the enthalpy changes at 298 K (room temperature) and C_p is the heat capacities of products (MgO, TiC, and TiB_2). The T_{ad} for Eq 1 was calculated using the Eq 4 and thermodynamic data (Ref 19) was found to be 3104 K which is much higher than the critical value of 1800 K. On the other hand, the specific heat generated in a metallothermic reaction dictates whether the reaction can self-propagate or not. The specific heat of a reaction is evaluated by dividing the reaction's enthalpy to the sum of the product's weight. If this value is between 2250 and 4500 J/g, the process results in a controlled and self-sustaining reaction (Ref 20). Specific heat value of Eq 1 was calculated to be 3676 J/g by using Factsage 5.3 thermochemistry software (Ref 21). Therefore, this reaction is self-sustaining, and these products could be synthesized from H_3BO_3-TiO_2-Mg-C system by a self-propagating combustion process.

Better understanding of the aforementioned processes can be obtained by examining a plot of the enthalpies of the reactants and products as a function of temperature. Such plots are often used to predict the properties of SHS processes (Ref 22, 23). Figure 7 has been drawn by Factsage software (Ref 21) that shows the total enthalpy of the reactants (upper line) and of the products (lower line) as a function of temperature. The steps correspond to the melting of the relevant components, H_3BO_3,

Mg, C, and TiO_2 in the case of the reactants and TiC, TiB_2, and MgO in the case of the products; evaporation is not included in the figure. The initial temperature is assumed to be 298 K. The horizontal line "A" represents adiabatic conditions. The adiabatic temperature would be given by its intersection with the line showing the enthalpy of the products. It is well beyond the melting points of all reactants. Although some heat is always lost to the environment, extensive melting is obvious from the macroscopic appearance of the products, especially after reactions with a large release of heat, i.e., with a large temperature increase. SEM on the product obtained by reducing TiO_2 with Mg found spherical particles, indicating the melting of even this highest-melting phase $\left(T_{m(TiO_2)} = 1843\ ^\circ C\right)$ (Ref 24). The heat loss may be much more dramatic in loose powder particles, but extensive melting is possible even in that case. Line "B," "C," and "D" of Fig. 7 is the schematic representation of a case when complete melting of TiO_2, Mg $(T_{m(Mg)} = 650\ ^\circ C)$ and H_3BO_3 $\left(T_{m(H_3BO_3)} = 139\ ^\circ C\right)$ take place. The line does not reflect the time dependence of the heat loss; consequently, the actual relationship need not to be a straight line. The presence of molten components can explain the propagation of the reaction in the loose powder. When the reaction starts through the collision of the components particles, local melting takes place. This fully or partially molten material collects solid reactant particles, and further reaction and melting take place. The ignition time is usually shorter than 30 s.

3.3 Leaching

The leaching process tests were carried out by using a solution of 2 M HCl at a temperature of about 90 °C for 30 min. It could be observed that with a complete MgO elimination, a small amount of TiB_2 is also dissolved which could be due to its small crystallite sizes (Ref 25, 26). MgO dissolution reaction in HCl acid solution is shown in Eq 5

$$MgO + 2HCl = Mg^{2+} + 2Cl^{-} + H_2O \qquad \text{(Eq 5)}$$

The solution was filtered after leaching and the purified products were washed by distilled water for several times to eliminate extra HCl acid until the pH value is about 7. At the end, the products were dried in air oven at 353 K for 1 h. Figure 8 shows the XRD patterns of the leached products which were synthesized at three different temperatures. It can be seen that the peaks due to MgO were almost completely eliminated as a result of the leaching process. On the other hand, increase of temperature leads to decrease in the amount of TiB_2. Because, similar to the higher milling time, in the higher temperatures, the reactivity of the reactants increases, resulting in a higher conversion of reactants to the side products. Williamson-Hall method was employed for XRD peaks analysis using following equation (Ref 27):

$$\beta_s \cos\theta = K\lambda/d + 2\varepsilon \sin\theta, \qquad \text{(Eq 6)}$$

where β_s is the sample broadening in radians, 2θ is the position of peak, K is the Scherrer constant [$K = 0.9$ (Ref 28)], λ is the x-ray wavelength ($\lambda = 1.54184$ Å), d is the crystallite dimension, and ε is an approximate upper limit of the lattice distortion. NBS640 sample (Si sample with free form defect and size broadening) was employed to remove instrument broadening (β_i) from XRD pattern. According to the following equation:

$$\beta_s^2 = \beta_e^2 - \beta_i^2, \qquad \text{(Eq 7)}$$

where β_e is the FWHM of the measured XRD peak. The average crystallite sizes of TiB_2 and TiC in the microstructure of the composite were calculated 40.7 and 75.6 nm, respectively, that were confirmed by TEM image. Figure 9 shows TEM micrographs of synthesized powder sample at the 900 °C after leaching (A_1). It is observed that, the products are made up of nanosized particles ranging from 30 to 90 nm.

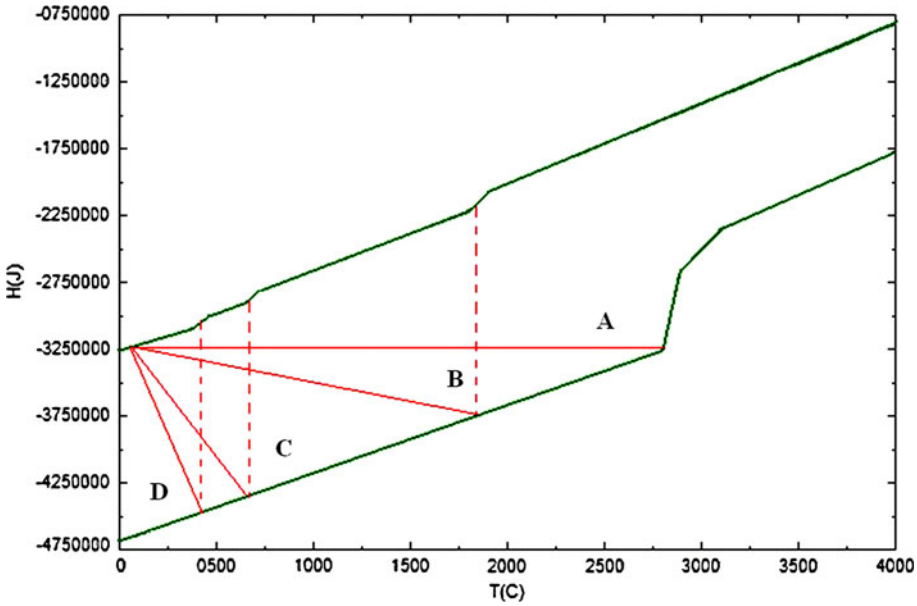

Fig. 7 The enthalpy of the reactants and the products as a function of temperature

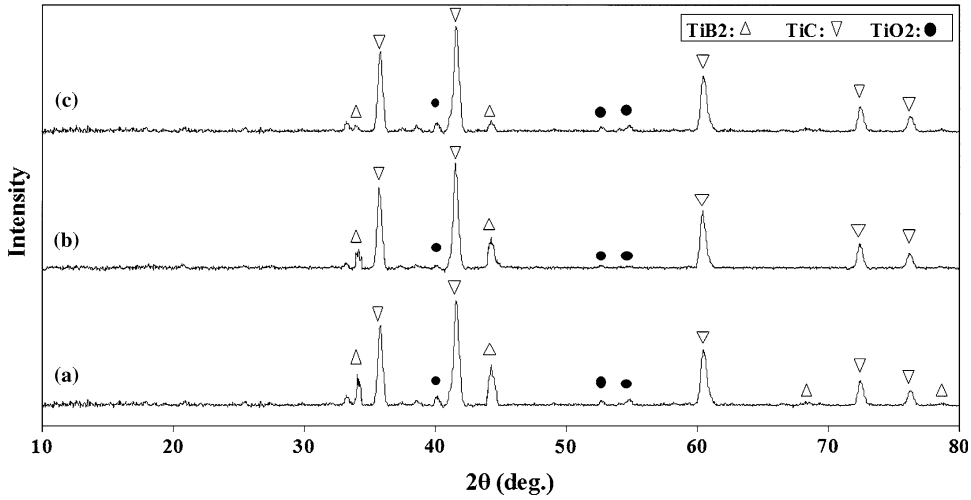

Fig. 8 XRD patterns of the leached samples synthesized in (a) 900 °C, (b) 1000 °C, and (c) 1100 °C

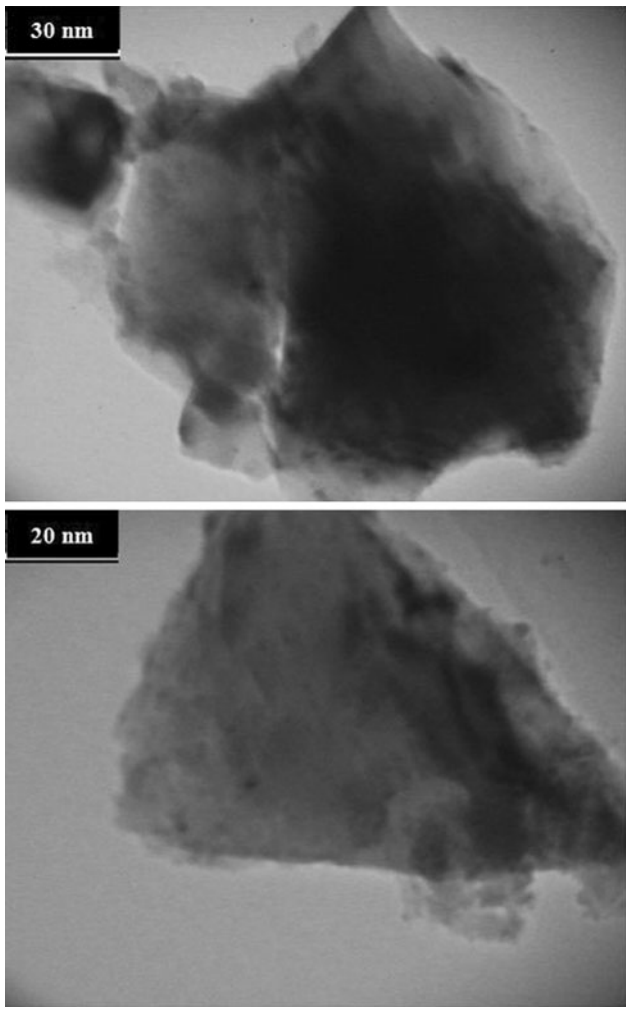

Fig. 9 TEM pictures of the leached samples in two magnifications

4. Conclusions

TiC-TiB_2 nanocomposite could be fabricated through MASHS process. XRD study showed that TiC and TiB_2 were not formed during milling process and ball milling for 0.5 h was found to be the optimum time for activation of the reactants. Characterization of the products samples after leaching with dilute acid showed that 900 °C is the optimum temperature for the synthesis of the nanocomposite. By using Williamson-Hall method, the average crystallite sizes of TiB_2 and TiC were calculated 40.7 and 75.6 nm, respectively, which were confirmed by TEM image.

References

1. A.W. Weimer, *Carbide Nitride and Boride Materials Synthesis and Processing*, Chapman and Hall, London, 1997, p 79–113
2. G. Wen, S.B. Li, B.S. Zhang, and Z.X. Guo, Reaction Synthesis of TiB_2-TiC Composites With Enhanced Toughness, *Acta Mater.*, 2001, **49**(8), p 1463–1470
3. J.J. Moore and H.J. Feng, Combustion Synthesis of Advanced Materials: Part I, Reaction Parameters, *Prog. Mater. Sci.*, 1995, **39**(4-5), p 243–273
4. S.C. Tjong and Z.Y. Ma, Microstructural and Mechanical Characteristics of In Situ Metal Matrix Composites, *Mater. Sci. Eng. A*, 2000, **29**(3-4), p 49–113
5. Y. Choi and S.W. Rhee, Synthesis of Dense Ceramic Particulate Reinforced Composites From Ni-Ti-C, Ni-Ti-B, Ni-Ti-B4C and Ni-Ti-C-B Systems Via the SHS Reaction, Arc Melting and Suction Casting, *J. Mater. Sci. Technol.*, 1995, **30**(1-2), p 4637–4644
6. H.Y. Wang, Q.C. Jiang, B.X. Ma, Y. Wang, and F. Zhao, Reactive Infiltration Synthesis of TiB_2-TiC Particulates Reinforced Steel Matrix Composites, *J. Alloys Compd.*, 2005, **391**(1-2), p 55–59
7. P. Mossino, Some Aspects in Self-Propagating High-Temperature Synthesis, *Ceram. Int.*, 2004, **30**(3), p 311–332
8. A.K. Khanra, L.C. Pathak, S.K. Mishra, and M.M. Godkhindi, Effect of NaCl on the Synthesis of TiB_2 Powder by a Self-Propagating High-Temperature Synthesis Technique, *Mater. Lett.*, 2004, **58**(5), p 733–738
9. E.T. Turkdogan, *Physical Chemistry of High Temperature Technology*, Academic Press, New York, 1980, p 5–24
10. F. Thevenot, Boron Carbide—A Comprehensive Review, *J. Eur. Ceram. Soc.*, 1990, **6**(4), p 205–225
11. J.H. Lee, C.W. Won, S.M. Joo, and D.Y. Maeng, Preparation of B_4C Powder from B_2O_3 Oxide by SHS Process, *J. Mater. Sci. Lett.*, 2000, **19**(11), p 951–954
12. V. Sundaram, K.V. Logan, and R.F. Speyer, Reaction Path in the Magnesium Thermite Reaction to Synthesize Titanium Diboride, *J. Mater. Res.*, 1997, **12**(4), p 2657–2664

13. U. Demircan, B. Derin, and O. Yucel, Effect of HCl Concentration on TiB_2 Separation From a Self-Propagating High-Temperature Synthesis (SHS) Product, *Mater. Res. Bull.*, 2007, **42**(2), p 312–318
14. C. Suryanarayana, Mechanical Alloying and Milling, *Prog. Mater. Sci.*, 2001, **46**(1-2), p 1–184
15. O. Yucel and M.A. Ozcelebi, Reduction Smelting of Bursa-Uludag Tungsten Concentrates by Aluminothermic Process, *Scand. J. Metall.*, 2000, **29**(3), p 108–113
16. R.M. German, *Liquid Phase Sintering*, Plenum Press, New York, 1985, p 225
17. F.W.J. Botta, R. Tomasi, E.M.J.A. Pallone, and A.R. Yavari, Nanostructured Composites Obtained by Reactive Milling, *Scr. Mater.*, 2001, **44**(1), p 1735–1740
18. Z.A. Munir, Synthesis of High Temperature Materials by Self-Propagation Combustion, *Am. Ceram. Soc. Bull.*, 1988, **67**(2), p 342–349
19. O. Kubaschewski and C.B. Alcock, *Metallurgical Thermochemistry*, 5th ed., Pergamon Press, Oxford, 1979
20. B. Derin, S. Ercayhan, and O. Yucel, *Proceedings of 10th International Ferroalloys Congress*, Cape Town, South Africa, 2004, p 78
21. C.W. Bale, A.D. Pelton, and W.T. Thompson, FactSage 5.4 Thermochemical Software for Windows™, Thermfact Ltd., Montreal, QC
22. J.A. Rodrigues, V.C. Pandolfelli, and W.J. Botta, Thermodynamic Predictions for the Formation of Ceramic-Metal Composites by a Self-Propagating High-Temperature Synthesis (SHS), *J. Mater. Sci. Lett.*, 1991, **10**(2), p 819–823
23. J.J. Moore and H.J. Feng, Combustion Synthesis of Advanced Materials: Part II. Classification, Applications and Modeling, *Progr. Mater. Sci.*, 1995, **39**, p 243–273, 275–316
24. L. Takacs, Reduction of Magnetite by Aluminum: A Displacement Reaction Induced by Mechanical Alloying, *Mater. Lett.*, 1992, **13**(2-3), p 119–124
25. N.J. Welham, Formation of TiB_2 from Rutile by Room Temperature Ball Milling, *Miner. Eng.*, 1999, **12**(10), p 1213–1224
26. R. Ricceri and P. Matteazzi, A Fast and Low-Cost Room Temperature Process for TiB_2 Formation by Mechanosynthesis, *Mater. Sci. Eng. A*, 2004, **379**(1-2), p 41
27. L. Lu, M.O. Lai, and C.W. Ng, Enhanced Mechanical Properties of an Al Based Metal Matrix Composite Prepared Using Mechanical Alloying, *J. Mater. Sci. Eng. A*, 1998, **252**(2), p 203–211
28. A.L. Ortiz and L. Shaw, X-ray Diffraction Analysis of a Severely Plastically Deformed Aluminum Alloy, *Acta Mater.*, 2004, **52**(8), p 2185–2197